14th International Symposium on Turbulence and Shear Flow Phenomena (TSFP14)
Heidelberg, Germany, July 28–31, 2026

HIGHLY RESOLVED SPATIO-TEMPORAL MEASUREMENTS OF THE NEAR-WALL TURBULENT PIPE FLOW UP TO RE_τ = 45 000

Christian Willert, Joachim Klinner
DLR Institute of Propulsion Technology
German Aerospace Center
51170 Köln, Germany
chris.willert@dlr.de · joachim.klinner@dlr.de

Daniel Schanz
Institute of Aerodynamics and Flow Technology
German Aerospace Center
37075 Göttingen, Germany
daniel.schanz@dlr.de

Lorenzo Magnani, Alessandro Talamelli, Gabriele Bellani
Department of Industrial Engineering / CIRI Aerospace
University of Bologna
Forlì, Italy
lorenzo.magnani9@unibo.it · alessandro.talamelli@unibo.it · gabriele.bellani2@unibo.it

ABSTRACT

A combination of low and high repetition 2d2c PIV measurements at a pixel magnification exceeding the viscous scale were performed in the near-wall region ($0 < y < 20\,\text{mm}$) of the turbulent pipe flow of the CICLoPE Long Pipe facility to extend upon similar measurements performed in 2016. The time-resolved imagery was processed with a multi-frame correlation scheme to achieve unprecedented velocimetry data with sub-viscous scale resolution. The acquired data base provides converged statistics of the velocity variances and at the same time yields corresponding spectral densities across a wide frequency range by combining data acquired at different sampling rates. Both the inner and outer streamwise turbulence peaks are captured with an underestimation at the highest shear Reynolds number of $\text{Re}_\tau = 44\,700$ caused by spatial filtering. The inner turbulence peak height follows the trend of Reynolds number dependent growth predicted by DNS and previous hot-wire measurements turbulent pipe flow but is lower than for flat plate boundary layer. Spectral densities in the near wall region were found to be essentially universal across the studied Reynolds number range. Further improvement is demonstrated by processing the images with a 2d Shake-the-Box (STB) Lagrangian particle tracking scheme.

INTRODUCTION

The long pipe in CICLoPE (Centre for International Cooperation in Long Pipe Experiments) is a world-unique facility operated by the University of Bologna for studying wall bounded turbulent flows and is capable of producing a high Reynolds number turbulent pipe flow ($Re_{\tau,\text{max}} \approx 50000$) at still measurable viscous scales in the 10 µm range. It consists of a 111.15 m long pipe of 901 mm diameter, where dynamically and thermally stable conditions can be provided (Talamelli *et al.*, 2009; Bellani & Talamelli, 2016).

The present turbulent pipe flow measurement campaign extends upon previous measurements performed by the authors in 2016 in the Framework of the EuHIT HoloPipe project (Willert *et al.*, 2017), and are aimed at improving convergence and extension to fully time-resolved 2d2c velocity data to facilitate spectral analysis of both streamwise and wall-normal velocity components.

EXPERIMENTAL TECHNIQUE

The high-speed particle image velocimetry (HS-PIV) measurement approach shown in Fig. 1 with corresponding photographs shown in Fig. 2 follows the same methodology initially introduced by Willert (2015). A high-speed camera (Vision Research T4040) is fitted with a telephoto macro lens (Nikon Micro Nikkor 200/4) and captures a narrow field of view (FOV) of ($1.5 \times 23.5\ \text{mm}^2$). The magnification was set to unity ($M = 1.00 \pm 0.01$) such that each camera pixel corresponds to 9.27 µm in physical space. This size slightly exceeds the viscous length scale at the highest Reynolds number ($l^* = \nu/u_\tau = 10.1\,\mu\text{m}$, see Table 1). The FOV was illuminated with a thin laser light sheet formed by the collimated beams of a dual resonator high-speed laser (Innolas/Iradion, Nanio Air, 2× 10 W), capable of providing laser pulses up to 400 kHz. For time-resolved, high-speed measurements camera frame rate and laser pulsing frequency were adjusted to produce particle image displacements of about 25 pixel at the centerline velocity. This ensured that the fastest particles were captured at least 5 times while transiting the field of view, thus enabling the possibility of tracking individual particle trajectories. Further measurements were acquired at lower camera framing rates (in frame-straddle mode) to capture a large number of nearly statistically independent velocity samples.

As outlined in Table 1, profile PIV measurements were performed at centerline velocities of $U_{cl} = 5\,\text{m/s}$ up to $50\,\text{m/s}$ spanning a shear Reynolds number range of $\text{Re}_\tau = 5500$ to 45 000. The quantity N_{eff} indicates the number of eddy turnover times computed as $N_{\text{eff}} = T_{acq}U_{cl}/R$, where T_{acq} is the total acquisition time for each case. As can be seen from Table 1, the number of eddy turnover times exceeds six-thousands for all Reynolds numbers, which is sufficient to bring the statistical uncertainty on the mean velocity below 1% for all cases and all wall positions. While this combination of time resolution and statistical accuracy is quite common for single-point techniques such as hotwire anemome-

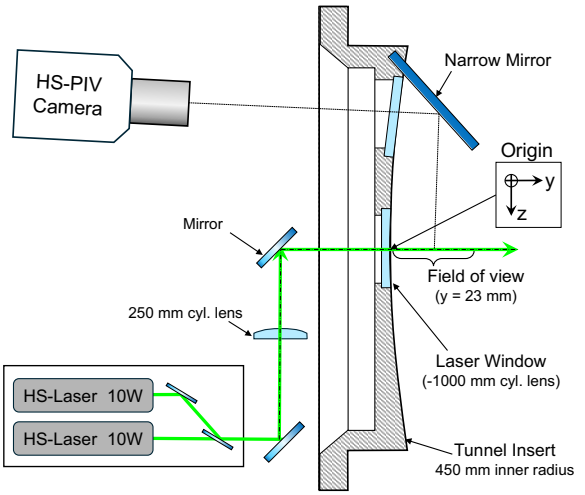

Figure 1. Schematic of the measurement setup for high-speed profile PIV on the test section of the CICLoPE Long Pipe facility.

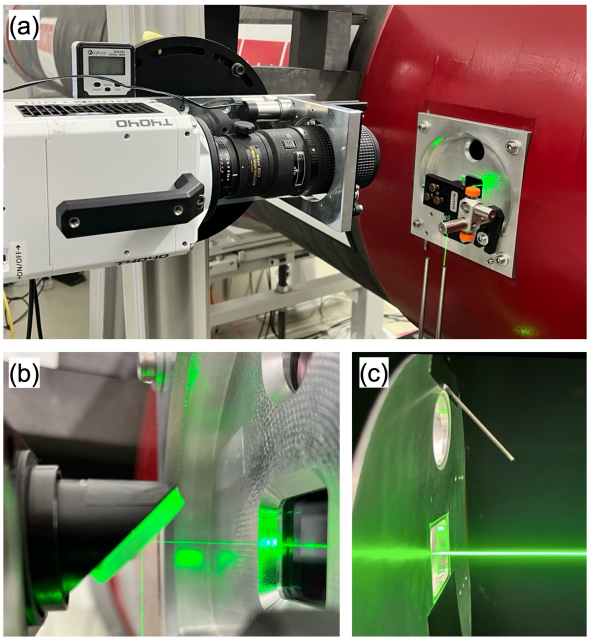

Figure 2. Photographs of the setup for high-speed profile PIV on the test section of the CICLoPE long pipe facility (a), (b) thin laser light sheet prior to entering the test section, (c) view of measurement domain inside the tunnel showing the thin laser light sheet and viewing mirror above.

try (HWA) and laser Doppler anemometry (LDA), it is indeed quite unique for multi-point, image-based measurements like PIV. The need for large sample counts is illustrated very clearly in Fig. 3 where each gray line represents the streamwise velocity variance $\langle uu \rangle$ for a time span of 0.23 s (25 638 images) corresponding to $N_{\text{eff}} = 15.5$ eddy turn-over times.

Figure 4 shows a pair of images acquired at the highest Reynolds number ($\text{Re}_\tau = 45\,000$, $U_{cl} = 50\,\text{m/s}$) and demonstrates the challenging imaging conditions at the glass surface. The scattered light not only varies between the two image frames but also changes over time such that a moving av-

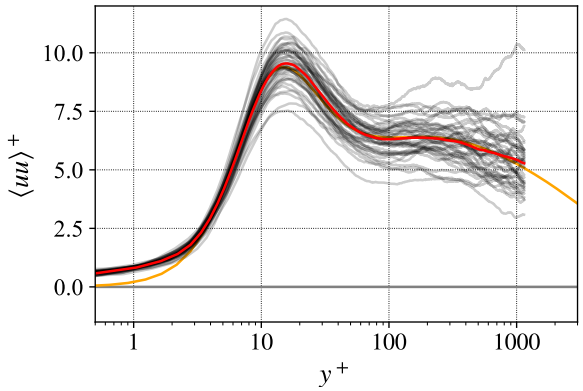

Figure 3. Profiles of the mean streamwise velocity variance $\langle uu \rangle$ for 42 image sequences, each with a duration of 0.23 s at $U_{cl} = 30\,\text{m/s}$ ($\text{Re}_\tau = 27\,700$).

erage is subtracted from each frame. This results in essentially flare-free images with significantly improved visibility of particles near the wall (see Fig. 4 c). Batch-processing was performed with a coarse-to-fine iterative cross-correlation algorithm (PIVview v.4.0, PIVTEC GmbH). The final interrogation sample size was set to 32×6 pixel corresponding to 300 µm in x and 55 µm in y. The resulting velocity records exhibit only mild pixel-locking artifacts (Fig. 5).

With increasing flow velocity the viscous scale reduces such that the finite size of the PIV sample size introduces spatial averaging effects (Segalini *et al.*, 2014). This is particularly noticeable at the highest Reynolds number, $\text{Re}_\tau = 44\,700$, for which the streamwise velocity variance $\langle uu \rangle$ is plotted in Fig. 6. At this Reynolds number the viscous scale matches the pixel scale such that a 6-pixel high sampling window results in a noticeable underestimation of the inner peak at $y^+ \approx 15$. While the reduction of the streamwise size of the sampling window results in a slightly increased peak value, the reduction of the sample's height from $5.6y^+$ to $2.8y^+$ (6 pixel vs. 3 pixel) shows a more pronounced effect. Noteworthy is the fact that the curves collapse common values with increasing wall distance which can be explained by the shift toward larger-scale energy containing structures away from the wall which are better resolved by PIV. Despite these limitations, these measurements nearly match the resolution ($l^+ \approx 20$) of the highest resolution hot-wire measurements made in the same facility (Fiorini, 2011; Zheng *et al.*, 2022), with the potential of further improvements if further particle-tracking schemes are applied.

RESULTS

Fig. 7 presents profiles of the streamwise velocity variance $\langle uu \rangle$ for all investigated Reynolds numbers, obtained by averaging the data from the individual records. The measurement data is referenced against DNS of a turbulent pipe flow at $\text{Re}_\tau = 12\,000$ (Pirozzoli, 2024) and indicates a good agreement. With increasing Reynolds number, the increase of energy in the outer region is clearly documented in Figure 7. This apparent maximum shifts towards higher y^+ values as the Reynolds number increases, in agreement with previous observations (Fiorini, 2011; Zheng *et al.*, 2022) where a logarithmic increase of the outer peak has been reported. For $\text{Re}_\tau > 15\,000$ a local minimum at $y^+ \approx 100$ is also observed.

The amplitude of the inner turbulence peak is plotted as colored symbols in Fig. 8 and includes data from the previous

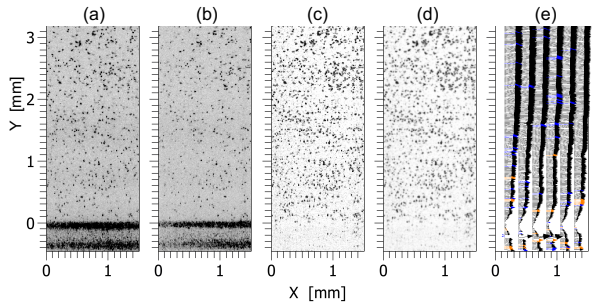

Figure 4. Near-wall detail of image pair (a,b) of 160 pixel width acquired at $U_{cl} = 50\,\mathrm{m/s}$ ($\mathrm{Re}_\tau = 44{,}700$), after background removal (c), low-pass filtering (d) and retrieved displacement data (e). Blue vectors are 2nd choice estimates, orange are interpolated outlier vectors.

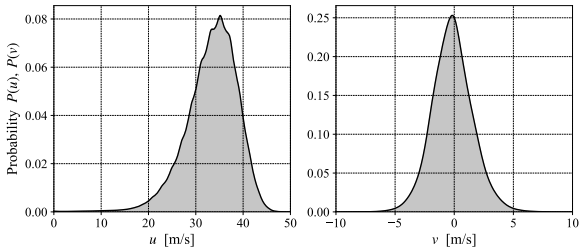

Figure 5. Probability distribution for both velocity components U,V at $U_{cl} = 50\,\mathrm{m/s}$ obtained from 42 velocity records of 0.5 s duration each (5.3×10^8 samples).

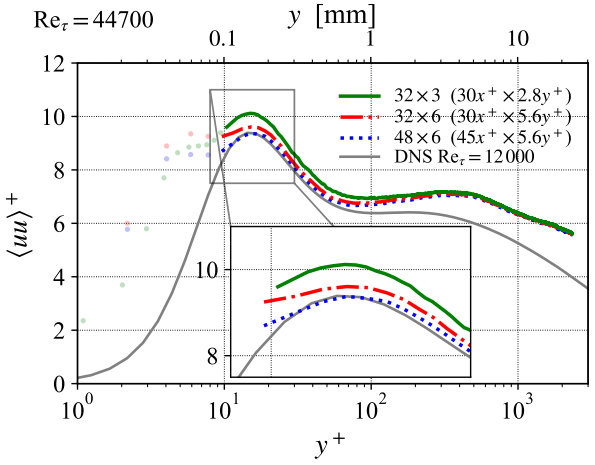

Figure 6. Effect of PIV sampling window size on the streamwise velocity variance $\langle uu \rangle$ at $U_{cl} = 50\,\mathrm{m/s}$ ($\mathrm{Re}_\tau = 44700$) obtained from 21 velocity records of 0.5 s duration.

measurement campaign by Willert *et al.* (2017) (open colored symbols). Essentially all data points fall short of the predicted amplitude introduced by Marusic *et al.* (2017) which is also the case for various DNS of turbulent pipe flow by Ahn *et al.* (2013, 2015) and Pirozzoli (2024). This difference may be rooted in the fact that the correlation introduced by Marusic *et al.* (2017) and – with slight variations – by Lee & Moser (2015) and Lozano-Durán & Jiménez (2014) are based on experiments and simulations of turbulent boundary layers and turbulent channel flows and do not include data for turbulent pipe flows.

The profiles of the wall-normal velocity variance $\langle vv \rangle$ and the co-variance $\langle uv \rangle$ (Reynolds shear stress) shown in Fig. 9 depart from the DNS-predicted profiles with increasing Reynolds number. The strongest discrepancy is present at the highest Reynolds number, $\mathrm{Re}_\tau = 44\,700$, and is a direct consequence of the PIV sampling window averaging across nearly 5 viscous length scales in the wall-normal direction and even larger distance in streamwise direction thereby attenuating the wall-normal fluctuations. This spatial filtering is also reflected by an increased attenuation of the peak turbulence intensity at the highest Reynolds numbers.

The good temporal resolution and long record lengths of the acquired data sets allow the estimation of the power spectral density (PSD) distribution across the vertical extent of the field of view. The 2d contour maps shown in Fig. 10 are assembled by plotting the individual spectra for each wall distance y side-by-side. To enhance the features of these maps the spectra are pre-multiplied by the frequency. In order to cover a large frequency range, the PSD maps are assembled by combining the spectra of the HS-PIV data with those obtained at the lower sampling frequencies. The "stitching" of the spectra causes minor discontinuities in the PSD maps of Fig. 10 that could be reduced by blending the adjoining sub-spectra. The resulting PSD representations differ from those reported in literature which commonly presents the data in wavenumber space rather than frequency space (see e.g. Fig.4 in Samie *et al.*, 2018). This can be achieved by a transformation using the mean velocity profile as the local convective velocity making use of Taylor's hypothesis of "frozen turbulence" (Taylor, 1938).

Fig. 10 shows the inner-scaled PSDs for three of the six investigated Reynolds numbers. First and foremost, the normalization results in nearly identical maps of the energy distribution across the acquired vertical domain ($0 < y < 20\,\mathrm{mm}$, $y/R < 0.045$) which is consistent with similar observations made by Samie *et al.* (2018) for the streamwise fluctuations u of a turbulent boundary layer and by Ono *et al.* (2025) for LDA measurements of a turbulent pipe flow.

The PSD of the streamwise fluctuations u (Fig. 10, top row) shows the inner spectral peak at a location coinciding with the wall-normal position of the maximum streamwise variance ($y^+ \approx 15$). The outer spectral peak appears in the region $10^{-3} < f^+ < 10^{-4}$ at a wall distance range of $100 < y^+ < 1000$.

The lower row of Fig. 10 shows the co-spectrum of the Reynolds shear stress ($\langle uv \rangle$). This quantity is measured with unprecedented accuracy and resolution in the near-wall region. These data, so far only available from DNS at lower Reynolds number, confirm y-scaling of the energy containing range, providing evidence of self-similarity of the Reynolds-stress producing eddies (see for example Baidya *et al.* (2017)).

OUTLOOK

While the post-processing of the extensive data set is still under way, the first assessment presented herein indicates a significant extension to the data base reported in Willert *et al.* (2017). In particular, the long duration records obtained at low sampling frequencies provides statistically converged data and at the same time complements the low frequency end of the PSDs as shown in Fig. 10. The present data also captures the second turbulence peak in the log-layer and may provide additional reference data to predict its evolution for $\mathrm{Re}_\tau > 50\,000$.

At present, the data collected at the highest Reynolds number ($\mathrm{Re}_\tau = 45\,000$) have been found to be strongly affected

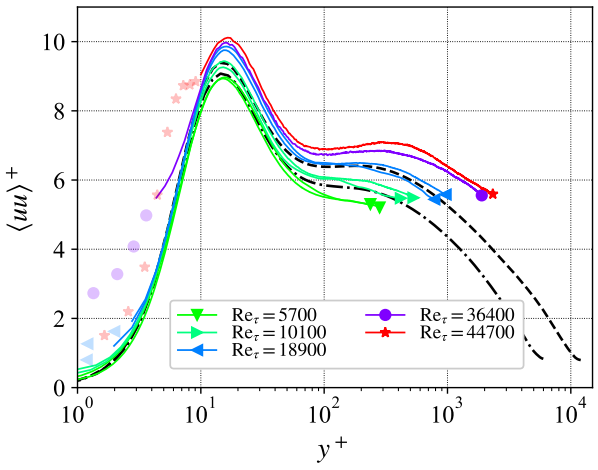

Figure 7. Profiles of the streamwise velocity variance $\langle uu \rangle$ for all investigated Reynolds numbers in viscous scaling. Faded symbols are represent under-resolved data points near the wall. Dashed/dotted lines indicates DNS prediction of turbulent pipe flow at $\mathrm{Re} = 6000$ ($-.$) and $\mathrm{Re} = 12000$ ($--$) by Pirozzoli (2024).

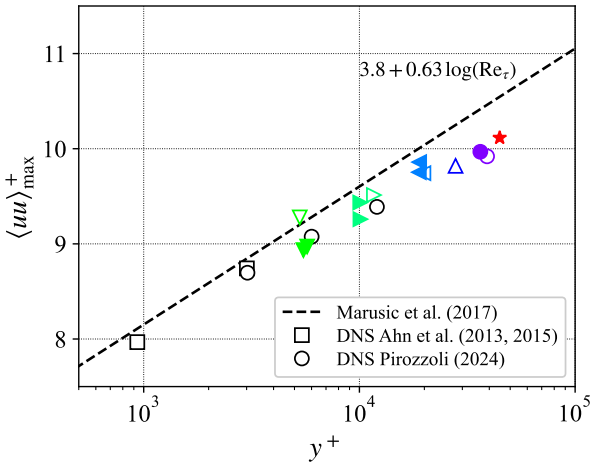

Figure 8. Reynolds number dependence of the maximum streamwise variance $\langle uu \rangle$ for all investigated Reynolds numbers with color-coding and symbols of Fig. 7. Open black symbols obtained from DNS of pipe flows by Ahn *et al.* (2013, 2015) (□), Pirozzoli (2024) (○). Dashed line according to prediction by Marusic *et al.* (2017).

by PIV-associated spatial filtering effects and suffer from increased laser flare near the wall such that the inner turbulence peak cannot be recovered. More elaborate processing schemes may mitigate the issue.

A further improvement of the data fidelity is expected by processing the acquired image sequences using a 2d variant of the *Shake-the-box* Lagrangian particle tracking algorithm (2D-STB, Schanz *et al.*, 2016). The method accounts for optical image aberration and the wall-normal motion of the FOV. As an example, velocity variances obtained at $\mathrm{Re}_\tau = 27,700$ are provided in Fig. 11. On average 3000-4000 particles were tracked for each time-step. Velocity profiles were determined from the Lagrangian particle tracks by averaging the particle properties in bins, spanning the full wall-parallel width with a wall-normal resolution of 1 µm.

From a measurement point of view the following observations and recommendations can be made:

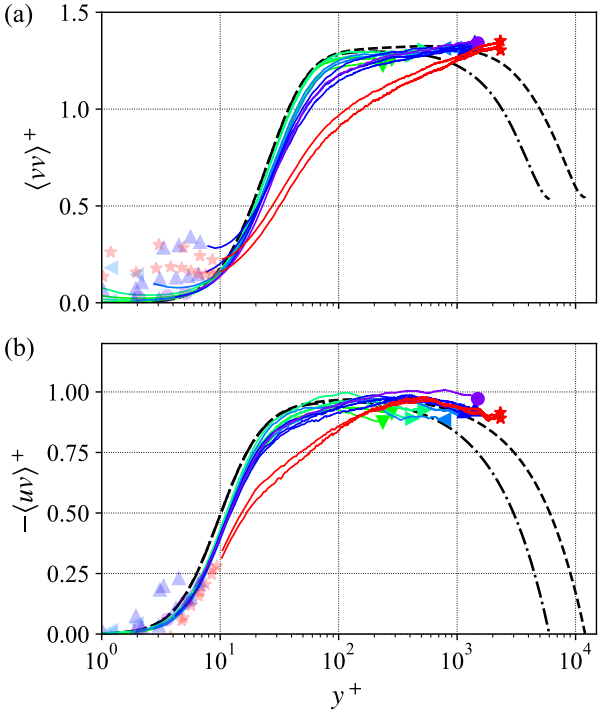

Figure 9. Profiles of the wall-normal velocity variance $\langle vv \rangle$ (a) and Reynolds shear stress $\langle uv \rangle$ (b). Color-coding and symbols corresponding to Fig. 7. Dashed/dotted lines indicates DNS prediction of turbulent pipe flow at $\mathrm{Re} = 6000$ ($-.$) and $\mathrm{Re} = 12000$ ($--$) by Pirozzoli (2024).

- Measurements in the immediate vicinity of the wall are challenged by the presence of laser flare and become increasingly relevant as viscous scales reduce with increasing Reynolds number.
- Spatial filtering effects becomes prevalent when the wall-normal sample size Δy exceeds the viscous scale $l^* = \nu/u_\tau$. This can be offset by further increasing image magnification.
- The multi-pulse measurement approach used for high-speed PIV improves the velocity estimation and facilitates the use of particle tracking velocimetry (PTV) schemes such as STB which outperforms conventional PIV based on image pairs.
- A multi-pulse measurement at the highest Reynolds number ($\mathrm{Re}_\tau = 45000$) with the present image magnification of unity would require a camera framing rate of $f_{\mathrm{acq}} \geq 220$ kHz. The herein utilized camera achieves 228 kHz at a reduced resolution of only 64 pixel lines. A particle moving at 50 m/s is associated with an image displacement of 24 pixel between exposures such that it would be imaged only 3 times which is insufficient for reliable PTV.
- To further improve the present measurements would require a camera with a framing rate of at least 250 kHz, ideally with a field of view wider than 64 pixels to capture a minimum four images of a passing particle. This frame rate must be even higher when the image magnification is further increased to offset the mentioned spatial filtering effects.

Table 1. PIV acquisition parameters for near-wall turbulent pipe flow measurements. PIV sample size: 32×6 pixel; light-sheet thickness $\approx 200\,\mu$m; number of effective samples N_{eff} based on eddy turn-over time $\tau = R/U_{\text{cl}}$.

Centerline velocity [m/s]	U_{cl}	**5.1**	**10.0**	**19.8**	**30.0**	**39.9**	**49.7**
Reynolds number	Re_τ	5 500	10 100	18 900	27 700	36 200	45 500
Friction velocity [m/s]	u_τ	0.193	0.347	0.650	0.950	1.25	1.54
Viscous scale [µm]	$l^* = \nu/u_\tau$	81.8	44.5	23.9	16.3	12.4	10.1
Effective PIV volume size	IW_{x^+}	3.63	6.67	12.4	18.2	23.9	29.4
	IW_{y^+}	0.7	1.3	2.3	3.4	4.5	5.5
	IW_{z^+}	2.5	4.5	8.4	12	16	20
HS-PIV sampling rate [kHz]	f_{acq}	20	40	80	110	150	(40)[1]
Laser pulse delay [µs]	Δt	50	25	12.5	9.09	6.67	4.5
	$\Delta t\, u_\tau^2\, \nu^{-1}$	0.12	0.19	0.34	0.53	0.67	0.67
Number of sequences		42	42	42	42	42	42
Samples per sequence	N_{HS}	25 638	25 638	25 638	25 638	42 591	20232
LS-PIV sampling rates [kHz]	f_{acq}	0.5 / 2	1 / 4	2 / 8	3 / 12	4 / 16	5 / 20
Number of sequences		4 / 4	4 / 4	4 / 4	8 / 8	8 / 8	4 / 4
Samples per sequence	N_{LS}	106 546	106 546	106 546	106 546	106 546	106 546
Independent samples	N_{eff}	6 600	6 500	6 400	12 400	7 500	6 500

[1] HS-camera is operated at a framing rate of 80 kHz

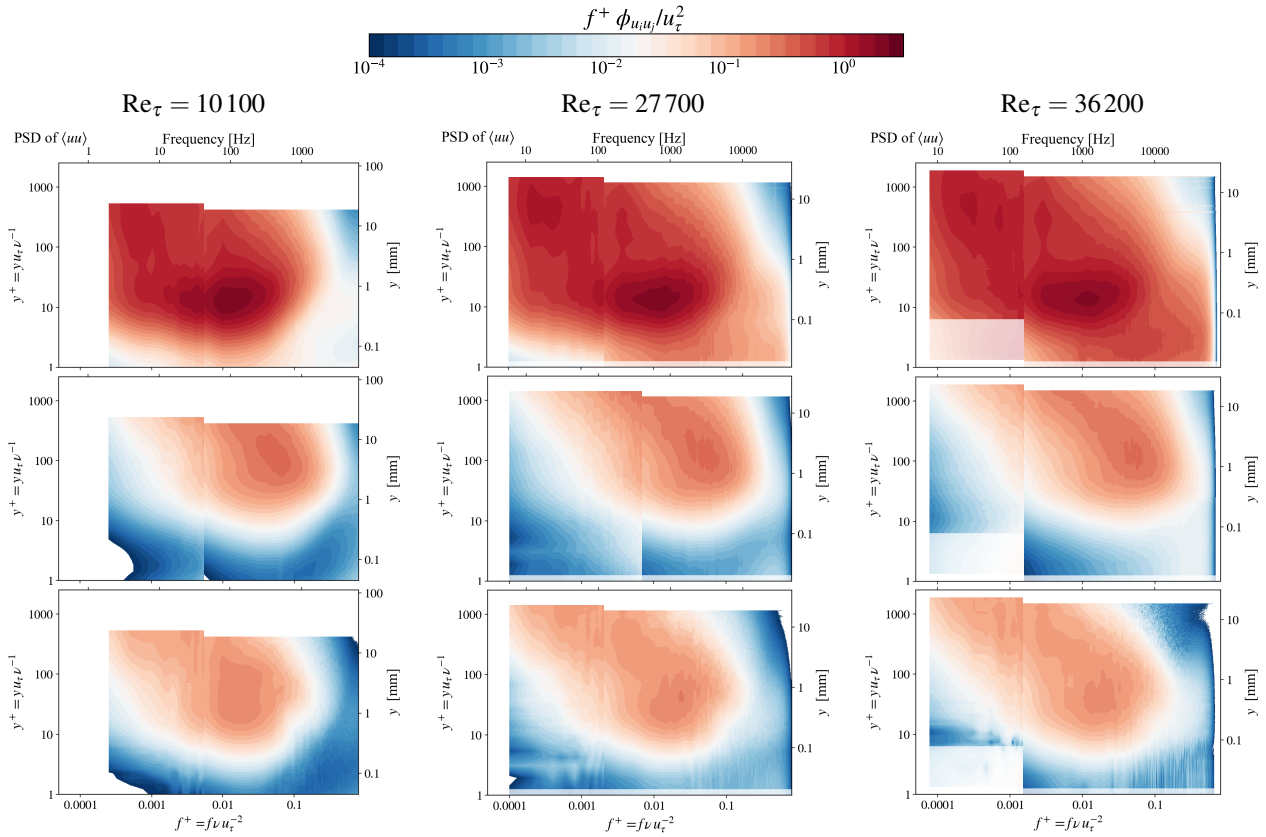

Figure 10. Pre-multiplied power spectral density at $\text{Re}_\tau = 10\,100$ (left column), $\text{Re}_\tau = 27\,700$ (middle column), $\text{Re}_\tau = 36\,200$ (right column) of the fluctuating streamwise velocity component u (top row), wall-normal component v (middle row) and the Reynolds shear stress $\langle uv \rangle$ (bottom row).

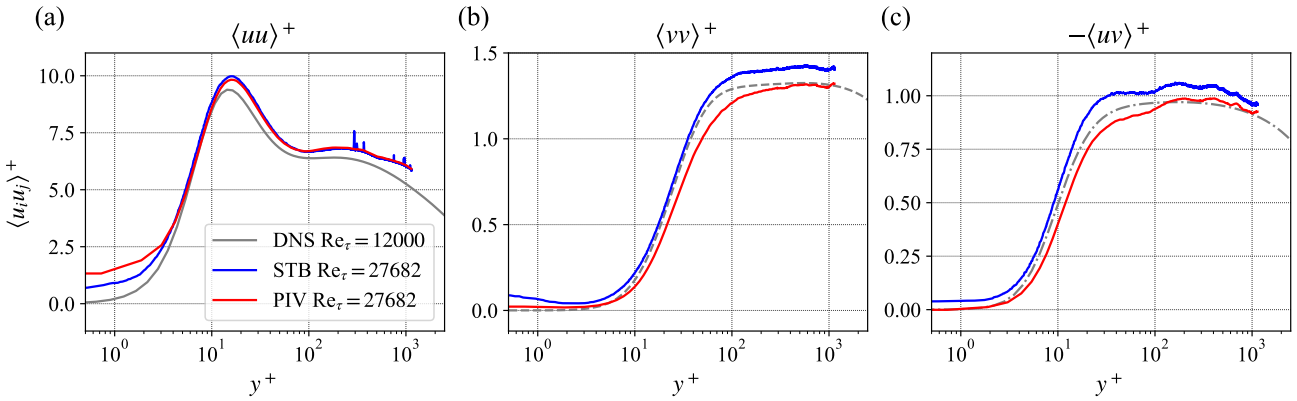

Figure 11. velocity variances determined at $\mathrm{Re}_\tau = 27\,000$ using cross-correlation processing (red) and 2D-STB (blue); DNS (gray) by Pirozzoli (2024); (a) variance of the streamwise component u, (b) wall-normal velocity variance, (c) Reynolds shear stress of $\langle uv \rangle$.

REFERENCES

Ahn, J, Lee, J H, Jang, S J & Sung, H J 2013 Direct numerical simulations of fully developed turbulent pipe flows for Res = 180, 544 and 934. *International Journal of Heat and Fluid Flow* p. 7.

Ahn, J, Lee, J H, Lee, J, Kang, J & Sung, H J 2015 Direct numerical simulation of a 30R long turbulent pipe flow at *Re* $_\tau$ = 3008. *Physics of Fluids* **27** (6), 065110.

Baidya, R., Philip, J., Hutchins, N., Monty, J. P. & Marusic, I. 2017 Distance-from-the-wall scaling of turbulent motions in wall-bounded flows. *Physics of Fluids* **29** (2), 020712.

Bellani, G. & Talamelli, A. 2016 The Final Design of the Long Pipein CICLOPE. *Springer Proceedings in Physics* pp. 205–209.

Fiorini, T. 2011 Turbulent Pipe Flow - High Resolution Measurements in CICLoPE. PhD thesis.

Lee, M. & Moser, R. D. 2015 Direct numerical simulation of turbulent channel flow up to $\mathrm{Re}_\tau \approx 5200$. *J. Fluid Mech.* **774**, 395–415.

Lozano-Durán, A. & Jiménez, J. 2014 Effect of the computational domain on direct simulations of turbulent channels up to *Re* $_\tau$ = 4200. *Physics of Fluids* **26** (1), 011702.

Marusic, I., Baars, W. J. & Hutchins, N. 2017 Scaling of the streamwise turbulence intensity in the context of inner-outer interactions in wall turbulence. *Physical Review Fluids* **2** (10), 100502.

Ono, M., Furuichi, N. & Tsuji, Y. 2025 Spectral distribution of three velocity components in high-Reynolds-number pipe flow using laser Doppler velocimetry measurements. *Physics of Fluids* **37** (5), 055134.

Pirozzoli, S. 2024 On the streamwise velocity variance in the near-wall region of turbulent flows. *J. Fluid Mech.* **989**, A5.

Samie, M., Marusic, I., Hutchins, N., Fu, M. K., Fan, Y., Hultmark, M. & Smits, A. J. 2018 Fully resolved measurements of turbulent boundary layer flows up to $\mathrm{Re}_\tau = 20\,000$. *Journal of Fluid Mechanics* **851**, 391–415.

Schanz, D., Gesemann, S. & Schröder, A. 2016 Shake-The-Box: Lagrangian particle tracking at high particle image densities. *Exp. Fluids* **57**.

Segalini, A., Bellani, G., Sardina, G., Brandt, L. & Variano, E. A. 2014 Corrections for one- and two-point statistics measured with coarse-resolution particle image velocimetry. *Experiments in Fluids* **55** (6), 1739.

Talamelli, A., Persiani, F., Fransson, J., Alfredsson, P. H., Johansson, A., Nagib, H., Rüdi, J-D., Sreenivasan, K. & Monkewitz, P. 2009 CICLoPE — a response to the need for high Reynolds number experiments. *Fluid Dynamics Research* **41** (2), 021407.

Taylor, G. I. 1938 The spectrum of turbulence. *Proceedings of the Royal Society of London. A. Mathematical and Physical Sciences* **164** (919), 476–490.

Willert, C. 2015 High-speed particle image velocimetry for the efficient measurement of turbulence statistics. *Exp. Fluids* **56** (1).

Willert, C., Soria, J., Stanislas, M., Klinner, J., Amili, O., Eisfelder, M., Cuvier, C., Bellani, G., Fiorini, T. & Talamelli, A. 2017 Near-wall statistics of a turbulent pipe flow at shear Reynolds numbers up to 40 000. *J. Fluid Mech.* **826**.

Zheng, X.and Bellani, G., Mascotelli, L., Örlü, R., Ianiro, A., Vila, C. S., Discetti, S., Serpieri, J., Raiola, M., Talamelli, A., Li, Ye & Jiang, N. 2022 Inter-scale interaction in pipe flows at high Reynolds numbers. *Experimental Thermal and Fluid Science* **131**, 110529.